Identification of a Novel Function of PiT1 Critical for Cell Proliferation and Independent of Its Phosphate Transport Activity*□S◆

Laurent Beck[‡§1,2], **Christine Leroy**[‡§1], **Christine Salaün**[‡§], **Germain Margall-Ducos**[§¶‖], **Chantal Desdouets**[§¶‖], **and Gérard Friedlander**[‡§]

From the [‡]*Growth and Signalling Research Center, INSERM, U845, F-75015 Paris, the* [§]*Cochin Institute, INSERM, U567, F-75015 Paris, the* [¶]*Cochin Institute, CNRS, UMR8104, F-75015 Paris, and the* [‖]*Faculté de Médecine, Université Paris Descartes, F-75015 Paris, France*

PiT1 is a Na$^+$-phosphate (P$_i$) cotransporter located at the plasma membrane that enables P$_i$ entry into the cell. Its broad tissue expression pattern has led to the idea that together with the closely related family member PiT2, PiT1 is the ubiquitous supplier of P$_i$ to the cell. Moreover, the role of P$_i$ in phosphorylation reactions, ATP production, DNA structure, and synthesis has led to the view that P$_i$ availability could be an important determinant of cell growth. However, these issues have not been clearly addressed to date, and the role of either P$_i$ or PiT proteins in cell proliferation is unknown. Using RNA interference in HeLa and HepG2 cells, we show that transient or stable PiT1 depletion markedly reduces cell proliferation, delays cell cycle, and impairs mitosis and cytokinesis. *In vivo*, PiT1 depletion greatly reduced tumor growth when engineered HeLa cells were injected into nude mice. We provide evidence that this effect on cell proliferation is specific to PiT1 and not shared by PiT2 and is not the consequence of impaired membrane Na$^+$-P$_i$ transport. Moreover, we show that modulation of cell proliferation by PiT1 is independent from its transport function because the proliferation of PiT1-depleted cells can be rescued by nontransporting PiT1 mutants. PiT1 depletion leads to the phosphorylation of p38 mitogen-activated protein (MAP) kinase, whereas other MAP kinases and downstream targets of mammalian target of rapamycin (mTOR) remain unaffected. This study is the first to describe the effects of a P$_i$ transporter in cell proliferation, tumor growth, and cell signaling.

PiT1 belongs to the inorganic phosphate (P$_i$) transporter (PiT)[3] family (Transport Classification Database (TCDB) Number 2.A.20) (1) comprising conserved symporters throughout all kingdoms that use either sodium or proton gradients to transport P$_i$. Well known examples of this family includes the *Neurospora crassa* Pho4 and *Saccharomyces cerevisiae* Pho89 or the *Escherichia coli* transporters PiTA and PiTB and *Arabidopsis thaliana* Pht2 (2). In mammals, the PiT family is comprised of only two members, PiT1 (SLC20A1) and PiT2 (SLC20A2), which were initially identified as receptors for retroviruses (3, 4) and were subsequently found to possess electrogenic Na$^+$-P$_i$ symporter activity (5).

Phosphate has a structural role in phospholipids of cell membranes, nucleoproteins, and nucleic acids. It forms high energy ester bonds (*e.g.* in adenosine triphosphate and guanosine triphosphate) and plays a central role in cellular metabolic pathways and signal transduction through covalent phosphorylation of proteins and lipids. For these reasons, P$_i$ is essential for many vital functions, including storage and liberation of metabolic energy, delivery of oxygen to the peripheral tissues, muscle contractility, electrolyte transport, neurological functions, and integrity of bone (6). The broad tissue distribution of PiT1 and PiT2 has led to the proposal that these transporters could serve a housekeeping role for cellular P$_i$ homeostasis (5, 7), although direct experimental evidence is lacking. Specifically, the consequences of variation of PiT expression at the cell surface on cell energy homeostasis and cell proliferation are not known. Moreover, although the consequences of variation of P$_i$ supply to the cell have been studied, P$_i$ starvation results in an up-regulation of PiT protein expression (5, 8). For this reason, starving the cells of P$_i$ may not adequately uncover any potential role of the PiT proteins in cell proliferation.

In this study, we addressed the question of whether PiT1 and/or PiT2 could modulate cell proliferation. Through an RNA interference approach, we show that reduced expression of PiT1 results in decreased P$_i$ transport and cell proliferation in HeLa and HepG2 cells. PiT1 depletion delayed cell cycle and impaired mitosis and cytokinesis. *In vivo*, injection of PiT1-depleted HeLa cells in nude mice results in reduced tumor growth. We generated PiT1 non-transporting mutants and showed that modulation of cell proliferation through PiT1

◆ This article was selected as a Paper of the Week.
□S The on-line version of this article (available at http://www.jbc.org) contains supplemental Movies 1–4.
[1] Both authors contributed equally to this work.
[2] To whom correspondence should be addressed: Centre de Recherche INSERM U845, Université Paris Descartes, Faculté de Médecine, 156 Rue de Vaugirard, F-75015 Paris. Tel.: 33-140615491; Fax: 33-143060443; E-mail: laurent.beck@inserm.fr.
[3] The abbreviations used are: PiT, inorganic phosphate transporter; hPIT, human PIT; mTOR, mammalian target of rapamycin; MAP, mitogen-activated protein; MAPK, MAP kinase; ERK, extracellular signal-regulated kinase; JNK, c-Jun N-terminal kinase; SAPK, stress-activated protein kinase; PCNA, proliferating cell nuclear antigen; FBS, fetal bovine serum; PBS, phosphate-buffered saline; GST, glutathione S-transferase; siRNA, small interfering RNA; shRNA, short hairpin RNA; RNAi, RNA interference; FACS, fluorescence-activated cell sorting; NPT, Na$^+$-P$_i$ cotransporters.

expression is independent from P_i transport into the cell and cannot be compensated by PiT2 overexpression. PiT1 depletion did not affect the ERK1/2, JNK, and mammalian target of rapamycin (mTOR) signaling pathways, whereas p38 mitogen-activated protein (MAP) kinase was overphosphorylated, although it does not appear to be instrumental to the PiT1-mediated effect on cell proliferation. This study is the first to demonstrate a direct role of PiT1 in cell proliferation, tumor growth, and cell signaling. Altogether, our data describe a novel function for PiT1, independent from its previously known transport activity. Discussion regarding PiT1 structure-function relationship in relation to this novel function is presented.

EXPERIMENTAL PROCEDURES

Culture Conditions, Transfections, and Growth Curves—HeLa cells were maintained in Dulbecco's modified Eagle's medium supplemented with 5% FBS. The HepG2 cell line was cultured in a medium consisting of Dulbecco's modified Eagle's medium/Ham's F12, supplemented with 5 mg/liter insulin, 3.5×10^{-7} M hydrocortisone hemisuccinate, 2 mM L-glutamine, and 10% FBS. HepG2 cells were seeded at 5×10^3 cells/cm^2, and medium was renewed every day. For siRNA and shRNA transfections, cells were seeded 24 h before the experiment in antibiotic-free medium at 3×10^5 or 5×10^5 cells/well in a 6-well plate, respectively. Cells were transfected with 10 nM siRNAs or 4 μg of plasmid using Lipofectamine 2000 in a serum-free medium. Four hours after transfection, 5% FBS was added to the medium. For growth curves, 25,000 cells were seeded in triplicate in 24-well plates. Cells were trypsinized and counted each day.

Production and Purification of an Anti-PiT1 Antibody—A 59-amino acid peptide sequence from the central intracellular loop of PiT1 was fused to GST or to thioredoxine-V5-His$_6$, expressed in BL21AI *E. coli* (Invitrogen), and purified from bacterial lysates on GSTrapFF columns (for GST-PiT1) or by using the HisTrap kit (for thioredoxine-PiT1-V5-His$_6$ fusion protein) as per the manufacturer's instructions (GE Healthcare). Rabbits were immunized against human GST-PiT1 peptide (CovalAb), and the anti-PiT1 antibody was purified from rabbit serum by incubating the serum with pieces of polyvinylidene difluoride membrane blotted with 250 μg of purified thioredoxine-PiT1-V5-His$_6$ protein. Elution was performed using 0.2 M glycine, pH 2, and the eluate was rapidly neutralized with 1 M Tris, pH 10. The purified anti-PiT1 antibody was diluted in Tris-glycine, pH 7.4, 50% glycerol, 0.1% bovine serum albumin.

RNA Interference—Transient inactivation of *PiT1* was assayed using siRNA SMARTpool® from Dharmacon (Chicago, IL) (catalog number L-007432-01) as per the manufacturer's instructions. Individual siRNA duplexes corresponding to the siRNA from the pool were then tested separately. Each individual siRNA gave comparable inactivation of *PiT1* expression. Subsequent experiments were conducted with 10 nM *PiT1* siRNA-A (5'P-UAUCAGUUCAGACCACU-UGUU-3') and siRNA-B (5'P-UAUCUAUGCUGGUUUC-CUC UU-3'). Transient reduction of *PiT2* expression was achieved using siRNA SMARTpool® from Dharmacon (catalog number L-007433-01) used at 10 nM, as per the manufacturer's instructions. si*CONTROL*™ non-targeting siRNA 1 and

si*GLO*™ RISC-free siRNA from Dharmacon were used as negative controls in transient transfection experiments. Stable knockdown of PiT1 expression was performed by cloning an shRNA corresponding to the sequence of siRNA-B into the pSUPER vector (9). The scramble sequence of shRNA-B was used as a negative control. HeLa cells were transfected with the pSUPER-shRNAs, plated at limiting density, and puromycin-resistant clones were picked, expanded, and tested for PiT1 expression. The data presented herein are from individual clones displaying at least an 80% knockdown of PiT1 expression. Experiments were performed with 3–4 independent stable transfectants, and the data presented illustrate representative clones.

Cloning of Human PIT1 and Site-directed Mutagenesis—Human *PIT1* was PCR-amplified from human kidney cDNA using the primers listed in Table 1. The PCR product was subcloned into pCR2.1 TA cloning vector (Invitrogen) and subsequently subcloned into the pcDNA6A expression plasmid (Invitrogen), in-frame with the V5 and His$_6$ C-terminal tags. The integrity of the construct was verified by sequencing. Site-directed mutagenesis was used to introduce three silent mutations in the *PiT1* sequence at the siRNA-B binding site to render the cDNA resistant to siPiT1-B cleavage (*PiT1-RNAiR*). The transport-deficient mutants of PiT1, S128A and S621A, were constructed by site-directed mutagenesis (QuikChange; Stratagene) from the *PiT1-RNAiR* construct. The sequences of the respective primers are listed in Table 1. The human *PIT2*-expressing plasmid used in this study was previously described (10).

Gene Expression and Quantification—Total RNA was isolated from cells and tissue using NucleoSpin RNA columns (MACHEREY-NAGEL). Northern analysis of total RNA (25 μg) from HeLa cells was performed as described previously (11). For PCR detection of Na^+-P_i transporters, RNA (2 μg) was reverse-transcribed with 200 units of M-MLV-RT (Invitrogen) and PCR-amplified using the primers listed in Table 1. PCR reactions contained $1\times$ reaction buffer, 0.2 mM dNTPs, 1.5 mM MgCl$_2$, 0.25 μM each primer, and 0.05 units/μl *Taq* (Invitrogen). Cycle conditions were 94 °C for 1 min of initial denaturation followed by 36 cycles of denaturation (94 °C, 15 s), annealing (Table 1), and extension (72 °C, 30 s). For gene quantification, RNA (2 μg) was reverse-transcribed with 200 units of M-MLV-RT (Invitrogen). Real-time PCR was performed using SYBR Green chemistry (Thermo Scientific) on an ABI Prism 7700 detection system. The glucuronidase gene was used as the reference gene, and expression differences were calculated as described previously (12). Primer sequences are listed in Table 1.

Phosphate Uptake Measurements—Transport of phosphate was measured as described previously (13). Apparent affinity constant (K_m) and maximal transport rate (V_{max}) were calculated by non-linear curve fitting, assuming Michaelis-Menten kinetics.

DNA and Actin Staining—Cells grown on coverslips were washed with PBS, fixed with 3% paraformaldehyde at 20 °C for 15 min, washed twice with PBS, and incubated for 10 min with 20 mM glycine. Cells were permeabilized in PBS, 0.1% saponin for 30 min at room temperature and washed three times in a drop of PBS/saponin. Actin was stained by incubating cells in a

TABLE 1
Primers used in this study

Application	Gene	Sense (5'-3')	Antisense (5'-3')	Amplicon size	Ta (°C)	Cycles
cloning	*PiT1*	TAAACAACCACTACTCCAGAGAATG	CATTCTGAGGATGACATATCTGAAG	2058	58	35
mutagenesis	*PiT1* (RNAiR mutant)	TGGACTTGAAAGAGGAAACGAGTATC GATAGCACCGTGAAT GGTG	CACCATTCACGGTGCTATCGATACT CGTTTCCTCTTTCAAGTCCA	N/A	60	18
	PiT1 (Ser128 mutant)	GTTTTTGAAGCTCCCTATTGCTGGTAC CCATTGTATTGTTGGTG	CACCAACAATACAATGGGTACCAG CAATAGGGAGCTTCAAAAAC	N/A	60	18
	PiT1 (Ser621 mutant)	TCAAATATTGGCCTTCCCATCGCTACA ACACATTGTAAAGTGGGC	GCCCACTTTACAATGTGTTGT AGCG ATGGGAAGGCCAATATTTGA	N/A	60	18
probe	*PiT1*	TACAACTCGACTCAAGGGCTACTG	TTTGGTTGCTGACGGCTTGA	802	55	35
	PiT2	CTCTCATGGCTGGGGAAGTTA	GAGATGGGCGATTTCACAGAG	724	55	35
	β-actin	GAGGCCCAGAGCAAGAGAGG	AAGTCCAGGGCGACGTAGCA	499	60	30
expression screening	*PiT1*	TTTCTGTGCCCTTATCGTCT	TTTGGTTGCTGACGGCTTGA	360	60	36
	PiT2	CTCTCATGGCTGGGGAAGTTA	GAGATGGGCGATTTCACAGAG	724	57	36
	Npt1	AGCCGAGTATGGAAATGGAT	TAGCCCAGACTGGAAGCGACT	807	56	36
	Npt2a	TCATCACAGAGCCCTTCACGA	GGAGATAGAGGACGGCAAACC	753	54	36
	Npt2b	CGCCAAATGCCAGCAT ATCTT	GTTGGAGCCCAGCGTGAGT	346	59	36
	Npt2c	GTGGCCCAGGTCGTGAGG	CCGGCCAGGTTGAAGAAGA	311	57	36
qPCR	*PiT1*	CAGCGTGGACTTGAAAGAGG	TGACGGCTTGACTGAACTGG	98	60	40
	PiT2	TCTCATGGCTGGGGAAGTTAGT	TTGCGACCAGTGAGAATCCTAT	131	60	40
	Npt1	TCTTCACAGCAGCAGGATTTCTC	TAAACACTCCACCCAAGCAAAG	138	60	40
	Npt2a	AGCCCCAGGGAGAAGCTGTC	CCACAGAAGGATACCCGAGA	81	60	40
	Npt2b	GCTGCCATCCCCATTATCAT	AAGAGCACCAACACGGACAG	158	60	40
	Npt2c	CCTGCTGGAGAGGCTAAGTG	CGCACCAGTGCTTAATGAGA	188	60	40
	Glucuronidase	CTCATTTGGAATTTTGCCGATT	CCGAGTGAAGATCCCCTTTTA	114	60	40

drop of Texas Red-X phalloidin (1:250) (Molecular Probes) for 30 min at 20 °C in the dark. Cells were washed three times in PBS and incubated in a drop of Hoechst 33342 (Sigma) at 2 μg/ml in PBS for 10 min at 20 °C in the dark to stain DNA. After the incubation, coverslips were washed twice in PBS to remove non-adherent cells, mounted in Glycergel mounting medium (Dako), and photographed under a microscope (Nikon Eclipse 800).

Time-lapse Video Microscopy—HeLa cells were cultured in Petri dishes equipped with glass coverslips and placed in a humidified and thermo-regulated chamber maintained at 37 °C on the stage of an inverted epifluorescence microscope (Axiovert 200, Carl Zeiss) equipped with a monochromatic light, a cooled CCD camera (ORCA, Hamamatsu Photonics), a motorized stage, a piezo z objective, and Plan-Apochromat 20×/0.75 NA and Plan-Neofluar 40×/0.75 NA objectives (Carl Zeiss). Images of dividing cells were acquired during 4–16 h at a frequency of one image each 2 min. MetaMorph software (Universal Imaging, West Chester, PA) was used for computer-based image acquisition and analysis of live cell data. The single images shown were prepared using Adobe PhotoShop® CS3.

Flow Cytometry Analysis and Synchronization of HeLa Cells—Cells were trypsinized and centrifuged at 1,000 × *g* for 5 min in a conical tube. Cell pellets were thoroughly resuspended in 0.2 ml of PBS, fixed by slowly adding them onto 1.8 ml of ice-cold 70% ethanol, and incubated for 3 h at 4 °C. For DNA content analysis, fixed cells were stained with 0.02 mg/ml propidium iodide in PBS containing 0.1% Triton X-100, 0.2 mg/ml DNase-free RNase A, for 30 min at 37 °C. Synchronization of HeLa cells

at G_1/S transition was performed by double thymidine block, as described previously (14). Every 2 h after drug release, cells were fixed in ice-cold 70% ethanol and stained with 0.02 mg/ml propidium iodide, and their cycle profile was analyzed by flow cytometry analysis on a BD Biosciences FACSCalibur flow cytometer with CELLQuest software.

Confocal Microscopy—Confluent cells were fixed, and the actin and/or expressed proteins were stained. Immunodetection of hPIT1 was performed using our custom antibody described in this study and a secondary anti-rabbit antibody coupled to fluorescein isothiocyanate. Coverslips were mounted on glass slides using glycerol (Dako) containing 2.5% 1.4-diazabicyclo-(2.2.2) octane (Sigma) as a fading retardant. Confocal images were taken by using a Leica TCSSP (Wetzlar, Germany) laser scanning microscope equipped with a ×63 oil immersion objective.

Immunofluorescence on Living Cells—Cells were seeded on slides and cultured overnight. Slides were washed with cold PBS and placed in 35 μl of PBS containing anti-V5 antibody (1:250) and 1% bovine serum albumin for 1 h at 4 °C in the dark. After four washes with cold PBS, cells were incubated as above with Alexa Fluor® 488 goat anti-mouse IgG (1:300 dilution) secondary antibody. Cells were washed with cold PBS and fixed in PBS containing 1% paraformaldehyde and 1% bovine serum albumin for 20 min at room temperature. Images were acquired under fluorescent illumination (Nikon Eclipse 800).

Immunoblot Analysis and Antibodies—Cells were detached and the cell pellet was incubated for 30 min in ice-cold lysis buffer (150 mM NaCl, 10 mM Tris-HCl, 5 mM EDTA, 1% Non-

idet P-40, 0.1% SDS, 0.5% deoxycholate, 1 mM Na_3VO_4, 1 mM NaF, 5 mM sodium pyrophosphate, 0.2 M phenylmethylsulfonyl fluoride, and a protease inhibitor mixture). After centrifugation at 14,000 rpm for 15 min, the protein extracts (supernatants) were boiled in $1\times$ SDS loading buffer prior to SDS-PAGE. Proteins were transferred to polyvinylidene difluoride membrane and blocked with 5% milk/TBST (10 mM Tris, 154 mM NaCl, 0.15% Tween 20) for 1 h. Blots were probed with primary antibodies in 5% bovine serum albumin or milk/TBST overnight followed by secondary antibodies for 1 h, detected using ECL Western blotting detection reagent, and exposed on ECL hyperfilm (GE Healthcare). Monoclonal anti-14-3-3σ clone CS112-2AB was from Upstate Biotechnology, mouse monoclonal anti-V5 antibody was from Invitrogen, and anti-bromodeoxyuridine antibody was from Amersham Biosciences. Monoclonal anti-β-actin clone AC-74 or anti-α-tubulin (Sigma) were used as loading controls. All other antibodies were from Cell Signaling Technology and are as follows: anti-p44/42 MAPK and anti-phospho-p44/42 MAPK (Thr-202/Tyr-204) antibodies to detect the ERK1/2 MAPK forms; anti-c-Raf and anti-phospho-c-Raf (Ser-259) antibodies; anti-SAPK/JNK and phospho-SAPK/JNK (Thr-183/Tyr-185) antibodies to detect JNK1/2/3; anti-p38 MAPK and anti-phospho-p38 MAPK (Thr-180/Tyr-182) antibodies; anti-p70 S6 kinase and anti-phospho-p70 S6 kinase (Thr-389) antibodies to detect S6K1 forms; anti-S6 ribosomal protein and anti-phospho-S6RP (Ser-240/Ser-244) antibodies; anti-4EBP antibody; and anti-Akt and anti-phospho-Akt (Ser-473) antibodies. All the antibodies were used according to the manufacturer's instructions.

Xenographic Growth of HeLa Tumor in Athymic Mice and PCNA Immunodetection—Outbred male athymic nude mice were obtained at 7 weeks of age from Elevage Janvier (Le Genest Saint Isle, France) and used for experiments at 8 weeks of age. Tumor formation was assayed by subcutaneously injecting 5×10^6 cells suspended in 100 μl of sterile PBS. Groups of five mice were injected at two sites per mouse. To measure the rate of tumor growth, the size of the tumor was monitored weekly using the formula: volume = (length $\times$ width^2)/2 (15). Mice and excised tumors were weighed 70 days after implantation (at time of sacrifice). Tumors were fixed in paraformaldehyde, and proliferating cell nuclear antigen (PCNA) immunodetection was performed using the M.O.M.™ immunodetection kit (Vector Laboratories) and anti-PCNA antibody (Dako), according to the manufacturer's instructions.

Statistics—All graphs are plotted as mean $\pm$ S.E. Statistics for dual comparisons were generated using Student's t tests, whereas statistics for multiple comparisons were generated using one-way analysis of variance followed by a suitable post hoc t test; *, $p < 0.05$, **, $p < 0.01$, for all statistics in the legends for Figs. 1 and 5–8.

RESULTS

The Na^+-P_i Transporter PiT1 Is Required for Proliferation of HeLa and HepG2 Cells—Quantification of Na^+-P_i transporter expression in HeLa cells using real-time PCR revealed that PiT1 and PiT2 were the only P_i transporters expressed in these cells (Fig. 1A). Other described mammalian P_i transporters, namely NPT1, NPT2a, NPT2b, and NPT2c (16), were not detected.
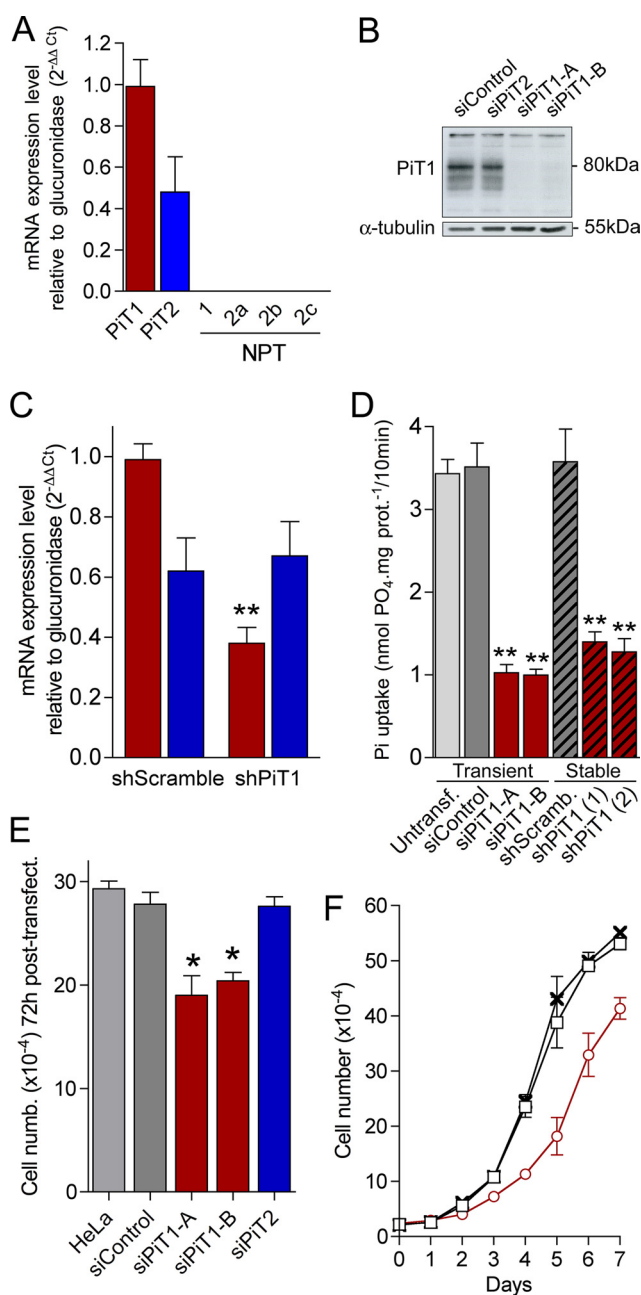
FIGURE 1. **PiT1, the major P_i transporter in HeLa cells, is critical for cell proliferation.** *A*, relative levels of Na^+-P_i cotransporters (NPT) mRNAs in HeLa cells were determined by real-time PCR. *PiT1* is most abundantly expressed in HeLa cells followed by that of *PiT2*; other *NPTs* are not detected. *Error bars* indicate S.E. *B*, transient inactivation of PiT1 in HeLa cells using siRNA. Proteins were extracted from HeLa cells transfected with 100 nM of the indicated siRNA, and PiT1 expression was analyzed by Western blot using anti-PiT1 antibody 48 h after transfection. *C*, depletion of PiT1 does not modify PiT2 expression, as measured by the relative mRNA expression levels (real-time PCR) of *PiT1* (*red bars*) and *PiT2* (*blue bars*) in shScramble or shPiT1 stably transfected HeLa clones. *D*, P_i transport was measured in transient and stable knockdown of PiT1 in HeLa cells. For transient knockdown of PiT1, HeLa cells were transfected with the indicated siRNA (10 nM) or untransfected (*Untransf.*), and P_i transport was determined 48 h after transfection. Stable shRNA clones were tested for P_i transport 4 days after seeding. **, $p < 0.01$. *E*, transient depletion of PiT1 reduces cell proliferation. HeLa cells were transfected with 10 nM of two different *PiT1*-specific siRNAs (*A* and *B*), a pool of *PiT2* siRNA, or untransfected. At 72 h after transfection, cells were counted. *Cell numb*, cell number. *, $p < 0.05$. *F*, the proliferation of stably PiT1-depleted HeLa cells is impaired. Untransfected HeLa cells (*crosses*) or HeLa cells stably transfected with PiT1 shRNA (*red circles*) or scramble shRNA (*white squares*) were grown in complete medium and counted on the indicated days.
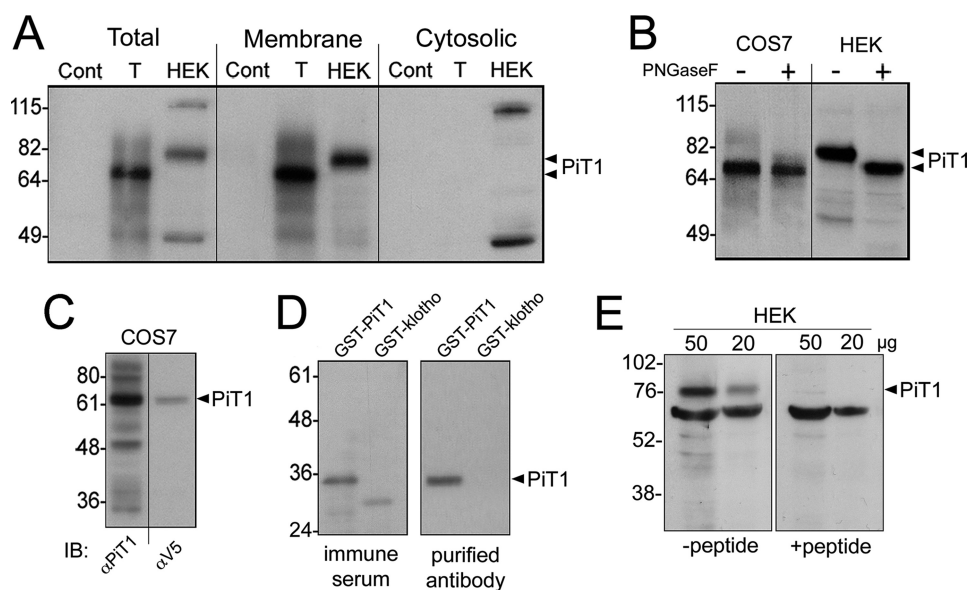
FIGURE 2. **Anti-PiT1 antibody production and characterization.** A polyclonal antibody against human PIT1 was generated as described under "Experimental Procedures." Briefly, a 59-amino acid peptide located in the intracellular loop of PiT1 was expressed as a GST fusion protein and used for immunization. Rabbit sera were then purified from anti-GST antibodies. *A*, total, membranous, and cytosolic protein extracts from untransfected (*Cont*; 1 μg of protein extract) or hPIT1-transfected (*T*; 1 μg) COS7 cells, as well as untransfected HEK cells (*HEK*; 20 μg of protein extract), were separated by SDS-PAGE, and the blotted membrane was probed with the purified anti-PiT1 antibody (1/500). *B*, glycosylation of endogenous *versus* transfected PiT1 protein. Proteins extracts from COS7 or HEK cells were treated (+) with 500 units of (*PNGaseF*) for 1 h at 37 °C or not treated (−) and then separated by SDS-PAGE, and the blotted filter was probed with the purified anti-PiT1 antibody (1/500). *C*, extracts from COS7 cells transfected with hPIT1-V5 were separated by SDS-PAGE, and the membranes were immunoblotted (*IB*) with either the anti-PiT1 (1/500) or the anti-V5 antibody (1/5000), as indicated. *D*, GST-PiT1 peptide used for immunization and an unrelated fusion peptide (*GST-klotho*) were separated by SDS-PAGE, and the blots were hybridized with immune serum or purified antibody, as indicated. *E*, competition with the immunogen peptide. Extracts from HEK cells (50 and 20 μg) were separated by SDS-PAGE, and the blotted filters were probed with anti-PiT1 (1/1000) antibody, which was preincubated for 1 h at room temperature with or without 0.5 μg of GST-PiT1 peptide, as indicated.

both in transient and in stable RNAi experiments, Na$^+$-P$_i$ transport function was reduced by 65–70% in HeLa cells (Fig. 1*D*). More detailed analysis of transport function reveals that the reduction in P$_i$ transport was due to a reduced transport capacity (V_{max}shScramble = 5.7 ± 0.3 nmol·mg of protein^{-1}; V_{max}shPiT1 = 2.4 ± 0.2 nmol·mg of protein^{-1}) rather than a change in transport affinity ($K_m$shScramble = 150 ± 16 μM; $K_m$shPiT1 = 132 ± 11 μM). Because PiT1 and PiT2 have the same affinity for P$_i$ (18, 19), the reduction in Na$^+$-P$_i$ uptake in HeLa cells is consistent with a decrease in PiT1 protein abundance at the cell membrane.

We next evaluated the effect of PiT1 knockdown on the proliferation of HeLa cells. Transient transfection of two different *PiT1* siRNAs led to a significant reduction in cell number, whereas unrelated siRNA (siControl) and *PiT2* siRNA had no effect on cell proliferation (Fig. 1*E*). Stable expression of *PiT1* shRNA showed that 4 or 5 days after equal seeding (*i.e.* at the time of exponential growth), the number of shPiT1 HeLa cells was half that of wild-type or shScramble HeLa cells (Fig. 1*F*). This result indicates that a wild-type level of PiT1 is necessary for normal proliferation of HeLa cells.

To exclude the possibility that the effect of PiT1-knockdown is specific to HeLa cells, PiT1 knockdown was performed in the non-tumorigenic HepG2 cell line, from hepatic origin. Expression analysis of the Na$^+$-P$_i$ transporters showed that although *PiT1* was the main transporter expressed in these cells, there was a high expression of *NPT1* and a weaker expression of *PiT2* (Fig. 4*A*). Stable inactivation of PiT1 using shRNA (Fig. 4*B*) resulted in reduced Na$^+$-P$_i$ transport due to a decrease in the transport capacity (V_{max}shScramble = 2.08 ± 0.16 nmol·mg of protein^{-1}; V_{max}shPiT1 = 1.31 ± 0.12 nmol·mg of protein^{-1}) rather than a change in the transport affinity ($K_m$shScramble = 75.1 ± 10.9 μM; $K_m$shPiT1 = 75.3 ± 15.3 μM) (Fig. 4*C*). Although the decrease in Na$^+$-P$_i$ transport following shPiT1 knockdown was less prominent than in HeLa cells, the proliferation of HepG2 cells was similarly affected, and the cell number was half that of shScramble HepG2 clones 4 days after seeding (Fig. 4*D*).

In HeLa Cells, PiT1 Depletion Delays the Cell Cycle and Impairs Mitosis and Cytokinesis—Hoechst staining of stably transfected shRNA HeLa clones revealed the presence of giant polyploid cells in the PiT1-depleted population and the frequent observation of lagging chromosomes in mitotic figures (Fig. 5*A*). A representative series of time-lapse images shows

PiT1 expression was 2.1-fold higher than *PiT2* in HeLa cells, in agreement with previous data obtained from cDNA microarrays hybridizations (17). The lack of expression of other P$_i$ transporters in HeLa cells, together with the fact that inoculation of nude mice with HeLa cells is a classical model of tumorigenesis, make them an attractive system for the study of PiT protein function. As shown in Fig. 1*B*, knockdown of *PiT1* expression in HeLa cells using two different siRNA constructs (siRNA-A and -B) was effective, as evidenced by Western blot analysis using a custom anti-PiT1 antibody (Fig. 2). More detailed analysis of RNAi-mediated knockdown of PiT proteins is presented in Fig. 3. Northern analysis showed that *PiT1* and *PiT2* siRNAs induce a specific knockdown of the respective transporter expression, with no compensatory up-regulation of the remaining PiT (Fig. 3, *A* and *B*). To study the prolonged effects of PiT1 inactivation, we generated an shPiT1 corresponding to the sequence of the siRNA-B and selected HeLa cell clones stably transfected with shPiT1-B plasmids. Real-time PCR data showed that in HeLa cells stably transfected by *PiT1* shRNA, *PiT1* mRNA expression was significantly decreased, whereas *PiT2* expression was unchanged (Fig. 1*C*). A similar reduction in PiT1 protein levels was seen with shRNA as with transient siRNA experiments (Fig. 3, *C* and *D*), and immunochemistry confirmed that plasma membrane labeling with anti-PiT1 antibody almost completely disappeared in HeLa cells stably transfected with *PiT1* shRNA (Fig. 3*E*). As a result,
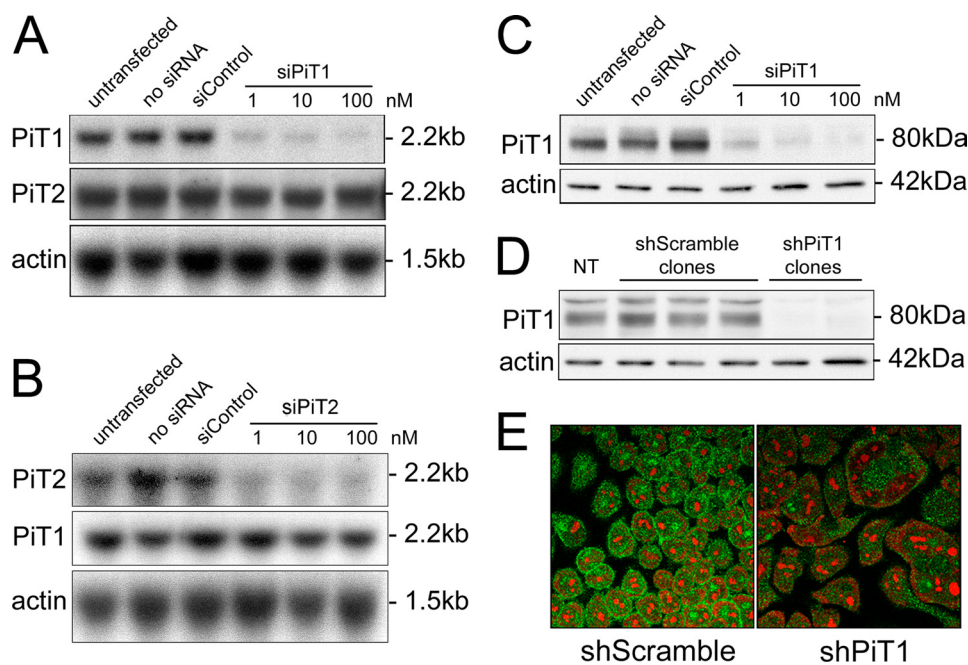
that a wild-type level of PiT1 is necessary for normal proliferation of HeLa cells.

FIGURE 3. **Inactivation of PiT1 and PiT2 in HeLa cells using RNAi.** *A* and *B*, transient inactivation of *PiT1* (*A*) and *PiT2* (*B*) using siRNA. RNA was extracted from untransfected, Lipofectamine control (*no siRNA*), siControl-transfected (100 nM), and siPiT1-transfected or siPiT2-transfected (1, 10, and 100 nM) HeLa cells. The effect of RNA interference was analyzed by Northern blot using *PiT1*, *PiT2*, and actin probes, as indicated. *C*, total proteins were extracted from untransfected, Lipofectamine control (*no siRNA*), siControl-transfected (100 nM), and siPiT1-transfected (1, 10, and 100 nM) HeLa cells. PiT1 expression was analyzed by Western blot using anti-PiT1 and anti-actin antibodies, as indicated. *D*, stable knockdown of PiT1 in HeLa cells using shRNA. Proteins from HeLa cells were extracted from untransfected (*NT*) cells or clones stably transfected with shScramble or shPiT1 in pSUPER vector, as indicated. PiT1 and actin expression were analyzed by Western blot using anti-PiT1 and anti-actin antibodies, as indicated. *E*, analysis of PiT1 expression in stably transfected shScramble and shPiT1 HeLa cells by indirect immunofluorescence. Cells were fixed, stained with propidium iodide, and labeled using an anti-PiT antibody and a secondary antibody coupled to fluorescein isothiocyanate. Confocal *x-y* sections of HeLa cells were taken, as indicated.

abnormal cytokinesis without cell separation, generating binucleated cells (Fig. 5*B* and supplemental Movie 1). Other figures of division show delayed progression through mitosis due to an extended metaphase stage (supplemental Movie 2) and generation of several nuclear poles (supplemental Movies 3 and 4), leading to either increased cell division duration or abnormal polyploid cells. In accordance with the reduced proliferation of PiT1-depleted HeLa cells, the mitotic index of shPiT1 clones was reduced by half (Fig. 5*C*). Mitotic figures were characterized by an increased proportion of cells in metaphase and a decreased proportion in anaphase and telophase, together with the appearance of numerous abnormal images of anaphase and telophase (Fig. 5*D*), consistent with the presence of polyploid cells in the PiT1-depleted population. FACS analysis of transiently or stably PiT1-depleted cells was characterized by a marked reduction in the proportion of PiT1-depleted cells in G_1 phase, together with an increase in S and G_2/M phases (Fig. 5*E* and Table 2), which, according to the reduction in the mitotic index, may indicate a delay in the G_2 phase. By synchronizing cells at G_1/S by double thymidine block (Fig. 5*F*), we found that entry in G_2/M was delayed in shPiT1 HeLa cells, consistent with our observations. A significantly higher proportion of cells in the PiT1-depleted cell population (16.5 *versus* 4.2%, when compared with HeLa cells) was still found in the G_2/M cell population (having 4n chromosomes) after synchronization (Fig. 5*F*), but they most likely represent tetraploid cells

arrested at the G_1/S transition (having two sets of 2n chromosomes). Pulse bromodeoxyuridine staining of asynchronous shScramble and shPiT1 HeLa cells showed that large polyploid PiT1-depleted cells were still cycling normally, whereas apoptosis end-stage terminal deoxynucleotidyltransferase-mediated dUTP-biotin nick end-labeling staining showed that these cells did not enter apoptosis more frequently than their normal counterpart (data not shown). Therefore, an increase in the apoptosis rate of these cells cannot account for the reduced number of cells seen after PiT1 depletion.

PiT1 Depletion in HeLa Cells Reduces Tumor Growth in Nude Mice—To evaluate whether PiT1 depletion affects tumor growth *in vivo*, nude mice were injected subcutaneously with shScramble, shPiT1 stably transfected HeLa cells, or parental HeLa cells (Fig. 6*A*). At 7 days after inoculation, all animals developed a palpable tumor at the injection site. However, the rate of tumor growth in the shPiT1 groups (two independent clones) was significantly slower than the control groups when comparing either tumor volume (Fig. 6*A*) or tumor size (Fig. 6*B*). This difference became significant ($p < 0.05$) by day 35. By day 70, the mean tumor size in shPiT1 mice was 0.41 ± 0.09 and 0.26 ± 0.07 cm^3, whereas in the control groups, it had reached 1.10 ± 0.13 and 1.4 ± 0.27 cm^3, corresponding to a 62–80% inhibition of tumor growth rate. Tumor weight was also decreased by 66–82% (Fig. 6*C*). Terminal deoxynucleotidyltransferase-mediated dUTP-biotin nick end-labeling staining of tumor sections revealed no difference in apoptotic cell number in the different tumors (not shown), whereas the number of PCNA-positive cells was much lower in shPiT1 HeLa cell-derived tumors (Fig. 6*D*). Taken together, these data indicate that reduced expression of PiT1 significantly inhibited tumor growth through decreased proliferation but did not affect tumor induction in nude mice.

Rescue of Cell Morphology, Proliferation, and Transport by RNAi-resistant PiT1 Mutants—Although we demonstrated, both in transient transfection with two different siRNAs and in stable transfection with separate shPiT1 clones, that depleting PiT1 from cells resulted in reduced proliferation, we conducted rescue experiments to rule out any possible off-target effects due to the RNA interference approach. To do this, we cloned the coding region of human *PIT1* into the pcDNA6 expression vector and mutated the target sequence of siRNA-B to produce a human *PIT1-RNAi*-resistant plasmid. HeLa cells stably transfected with shPiT1 were transfected with *PiT1-RNAiR* or
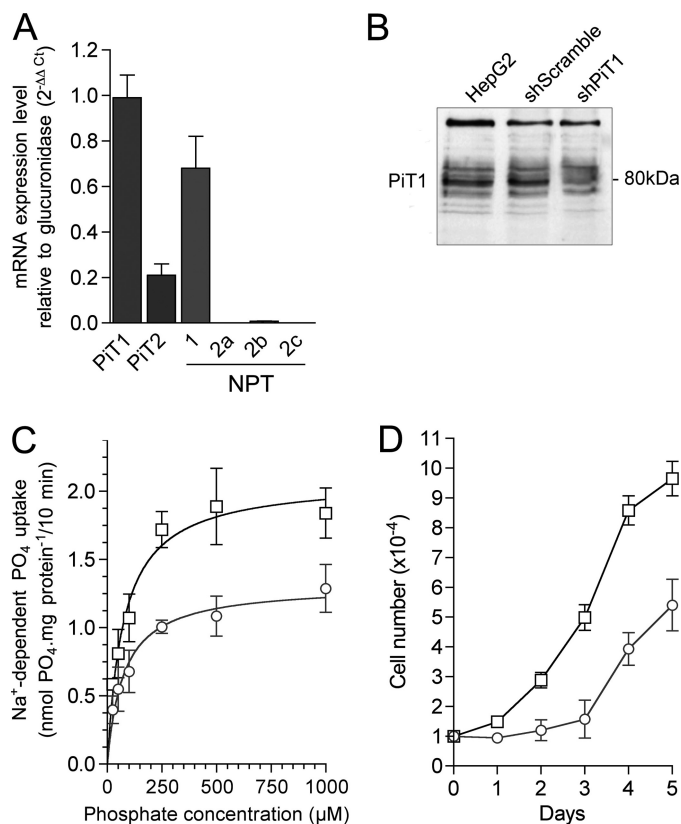
FIGURE 4. **Knockdown of PiT1 in HepG2 cells leads to reduced P$_i$ transport and impaired proliferation.** *A*, relative levels of NPT mRNAs in HepG2 cells using real-time RT-PCR reveals that *PiT1* and *NPT1* transporters are most abundantly expressed in HepG2 cells followed by that of *PiT2*; other *NPTs* are not significantly detected. *Error bars* indicate S.E. *B*, stable knockdown of PiT1 in HepG2 cells using shRNA. Proteins from HepG2 cells were extracted from untransfected cells (*HepG2*) or clones stably transfected with shScramble or shPiT1 in pSUPER vector, as indicated. PiT1 expression was analyzed by Western blot using anti-PiT1 antibody. *C*, Na$^+$-dependent P$_i$ uptake in shScramble (*square*) and shPiT1 (*circle*) HepG2 cells were calculated by subtracting uptake measured under Na$^+$-free conditions from that observed in the presence of Na$^+$ at each KH$_2$PO$_4$ concentration. *D*, HepG2 cells were grown in complete medium, stably transfected with shScramble (*square*), or shPiT1 (*circle*), and proliferation was assessed by counting the cells on the indicated days.

empty pcDNA6 plasmids and were grown in selective medium. As shown in Fig. 7A, expression of *PiT1-RNAiR* in shPiT1 HeLa cells rescued their cell morphology. The number of polyploid cells was low and not different from shScramble HeLa cells. These rescued cells appeared to have a restored proliferation rate, similar to that of shScramble HeLa cells (Fig. 7B). Moreover, the rescued cell morphology and proliferation was accompanied by a rescue of Na$^+$-P$_i$ transport (Fig. 7C). These experiments demonstrate that expressing sufficient PiT1 levels in the cells is enough to restore normal cell morphology, cell proliferation, and Na$^+$-P$_i$ transport. However, this does not show whether or not the transport function of PiT1 *per se* is instrumental in this rescue.

PiT1 Modulates Cell Proliferation Independently of Its Transport Function—Because the main reported role of PiT1 is to couple inward P$_i$ uptake to the Na$^+$ gradient across the cell plasma membrane (27), we evaluated whether this function underlies the effect of PiT1 knockdown on cell proliferation. To test this hypothesis, we attempted to rescue the proliferation of PiT1-depleted HeLa cells by transfecting a plasmid encoding

for human PiT2 in these cells. As shown on Fig. 8*A*, and in contrast to the results obtained with *PiT1-RNAiR* (Fig. 7), cell proliferation of shPiT1 HeLa cells could not be rescued by PiT2 (Fig. 8*A*), although PiT2 overexpression resulted in a significant increase in Na$^+$-P$_i$ transport (Fig. 8*B*). This result demonstrated that restoring a normal P$_i$ transport in shPiT1 HeLa cells is not sufficient to rescue a normal proliferation and suggests that PiT1 mediates its effects on cell proliferation independently from its transport activity. To test this hypothesis, we generated PiT1 mutants (using the *PiT1-RNAiR* backbone) in which the serines at position 128 or 621 were replaced by alanine residues (see Fig. 10*A*). This strategy was based on previous structure-function studies conducted on human PIT2 in which corresponding serine 113 and 593 were shown to be essential for Na$^+$-P$_i$ transport activity and did not affect protein expression and plasma membrane localization (20). As expected, despite adequate cell membrane localization and expression levels identical to that of wild-type PiT1 (see Fig. 10, *B* and *C*), the S128A mutant of PiT1 did not transport P$_i$ and hence was unable to rescue normal P$_i$ transport in PiT1-deficient cells (Fig. 8*B*). Despite the lack of Na$^+$-P$_i$ transport function, transient transfection of the S128A mutant in PiT1-deficient HeLa cells restored cell proliferation to a level identical to that observed in their wild-type counterpart (Fig. 8*C*). These results clearly show that PiT1, but not PiT2, selectively modulates cell proliferation, independently of its transport function.

Increased Phosphorylation of p38 MAPK in PiT1-depleted HeLa Cells—Because PiT1 Na$^+$-P$_i$ activity *per se* is not involved in the phenotype seen in shPiT1 cells, we questioned whether the knockdown of PiT1 could change the phosphorylation status of several signaling pathways implicated in cell proliferation. mTOR is a kinase that integrates signals from nutrients and growth factors to regulate cell growth and cell cycle progression coordinately. It is known to regulate translation mainly through the S6K1 (ribosomal protein S6 kinase 1) and the 4EBP1 proteins (eukaryotic translation initiation factor 4E-binding protein 1) (21). Study of the phosphorylation of S6, S6K1, and 4EBP1 in basal culture conditions, after starving of serum or restimulation, did not detect any differences between cells transfected with siControl, siPiT1, or siPiT2 siRNAs, suggesting that the mTOR pathway was unaffected (Fig. 9*A*). Similarly, as shown in Fig. 9*B*, depletion of PiT1 in HeLa cells affected neither the phosphorylation of the ERK (extracellular signal-regulated kinase) protein nor the phosphorylation of other components of the cascade such as c-Raf and 14-3-3σ. This was true in our basal culture conditions or after stimulation with either serum or 10 nM epidermal growth factor (*EGF*). The same observation was made for phosphorylation of the JNK MAPK (Fig. 9*B*). In contrast, significant changes were observed in the phosphorylation status of p38 MAPK under basal culture conditions as well as following serum stimulation (Fig. 9*C*). In PiT1-depleted cells, the phosphorylation status of p38 was strongly increased when compared with control cells, whereas the total amount of p38 protein was not changed. Importantly, phosphorylation of p38 was unaffected following transfection of the cells by a *PiT2* siRNA (Fig. 9*C*), showing that increased phosphorylation of p38 was not due to a decrease in Na$^+$-P$_i$
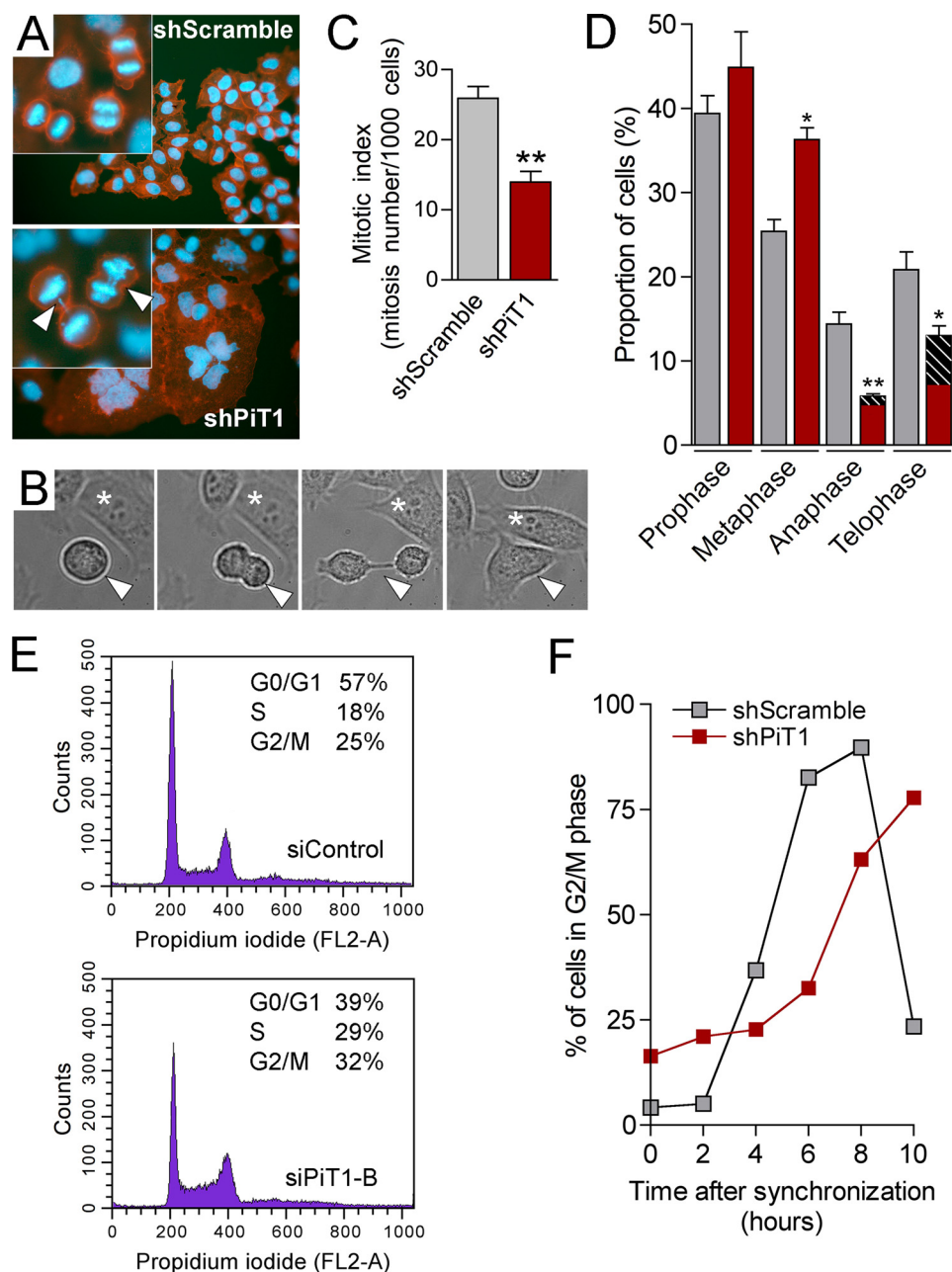
FIGURE 5. **Impaired cytokinesis and delayed cell cycle in PiT1-deprived HeLa cells.** *A*, Hoechst staining of HeLa cells in culture demonstrates polyploidic nucleus, increased cell size, and numerous lagging chromosomes (*arrows*) in shPiT1 HeLa cells. *B*, representative images of live cell imaging of shPiT1 HeLa cells. Cells were followed from prophase until the completion of mitosis. Note the failure of cytokinesis leading to a binucleated cell (*triangle*). The cell noted with the *asterisk* serves as a control. *C*, mitotic index of asynchronous mitotic PiT1-depleted HeLa cells was reduced by half. **, $p < 0.01$. *D*, mitotic figures were characterized by an increase of cells in metaphase and aberrant figures of anaphase and telophase (*hatched black bars*). *Error bars* indicate S.E. *, $p < 0.05$, **, $p < 0.01$. *E*, FACS analysis of HeLa cells transiently depleted from PiT1. Cells were transiently transfected with 10 nM control (*upper graph*) or *PiT1* (*lower graph*) siRNA. Forty-eight hours after transfection, asynchronous cells were stained with propidium iodide, and their DNA content was determined by FACS analysis. The percentages of cells in the respective phases are shown. *F*, entry in G_2/M phase was delayed in shPiT1 HeLa cells, as measured from cell populations synchronized at G_1/S by double thymidine block.

shown). We confirmed these data by knocking down p38 RNA synthesis using 100 mM p38 siRNA, arguing against a direct role of p38 in the PiT1-mediated effect on cell proliferation.

DISCUSSION

In this work, we have identified a novel function of PiT1 that is related to cell proliferation and is independent from its previously known Na^+-P_i transport activity. Our results further indicate that PiT2, the second member of the mammalian PiT family, does not share this function. We propose that this function may represent one of the main physiological roles of PiT1 and that sequence-specific regions of the PiT1 protein could underlie the differences observed between PiT1 and PiT2 protein function (Fig. 10).

P_i supply to the mammalian cell relies on the activity of the ubiquitously expressed Na^+-dependent P_i cotransporters PiT1 and PiT2, which utilize the Na^+ electrochemical gradient as the driving force to mediate the uphill import of P_i. Given the combined role of P_i in cellular processes and the function of PiTs as ubiquitous suppliers of P_i to the cell, we addressed the question of the role of these transporters in cell proliferation. In the course of our study, we showed that under normal physiological conditions and with an unchanged P_i availability to the cell, PiT1 expression was instrumental to cell proliferation. To our knowledge, this is the first observation that a Na^+-P_i transporter is directly involved in regulating cell proliferation. More importantly, we were able to dissociate the Na^+-P_i transport activity of PiT1 from its effect on cell proliferation, revealing a new distinct function for this membrane protein. This result is of fundamental importance because it opens new avenues on the physiological relevance of such transporters.

It has long been known that the membrane potentials in nonexcitable cells fluctuate during their progression through the cell cycle (for review, see Ref. 22). Typically, hyperpolarized somatic cells do not undergo mitosis, whereas developing and cancerous cells tend to be depolarized and mitotically active

transport. To gain insight into the possible link between PiT1 and p38 phosphorylation, we monitored the proliferation of PiT1-depleted HeLa cells in the presence of 2.5–20 μM p38 inhibitors SB202190 and SB203580. The results show that under these conditions, the proliferation rate of PiT1-depleted HeLa cells was not restored to wild-type levels (data not

TABLE 2

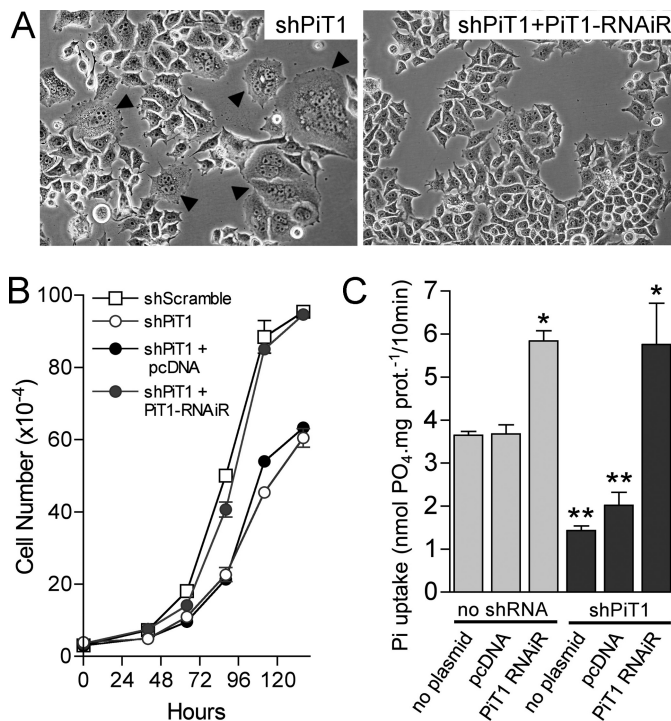**FACS analysis of HeLa cells transiently or stably depleted from PiT1**

For transient transfection, cells were transiently transfected with 10 nM siControl, siPiT1, or siPiT2 siRNA. Forty-eight hours after transfection, asynchronous cells were stained with propidium iodide, and their DNA content was determined by FACS analysis. For stable transfection, the DNA content was determined by FACS analysis of asynchronous stable HeLa cell clones stably transfected with the indicated shRNAs, which was determined 48 h after seeding. Results are expressed as the percentage of cells in the respective phase. *, $p < 0.05$ versus siControl or shScramble.

Transfection	siRNA	G_{0/G_1}	S	$G_{2/M}$
		%	%	%
Transient	siControl	56.8	18.1	25.1
	siPiT1-A	43.7*	28.8*	27.5
	siPiT1-B	39.4*	28.7*	31.8*
	siPiT2	56.6	16.2	27.2
Stable	shScramble 1	68.0	15.3	16.6
	shScramble 2	68.6	15.2	16.2
	shPiT1 1	50.2*	23.8*	26.0*
	shPiT1 2	43.0*	27.8*	29.2*
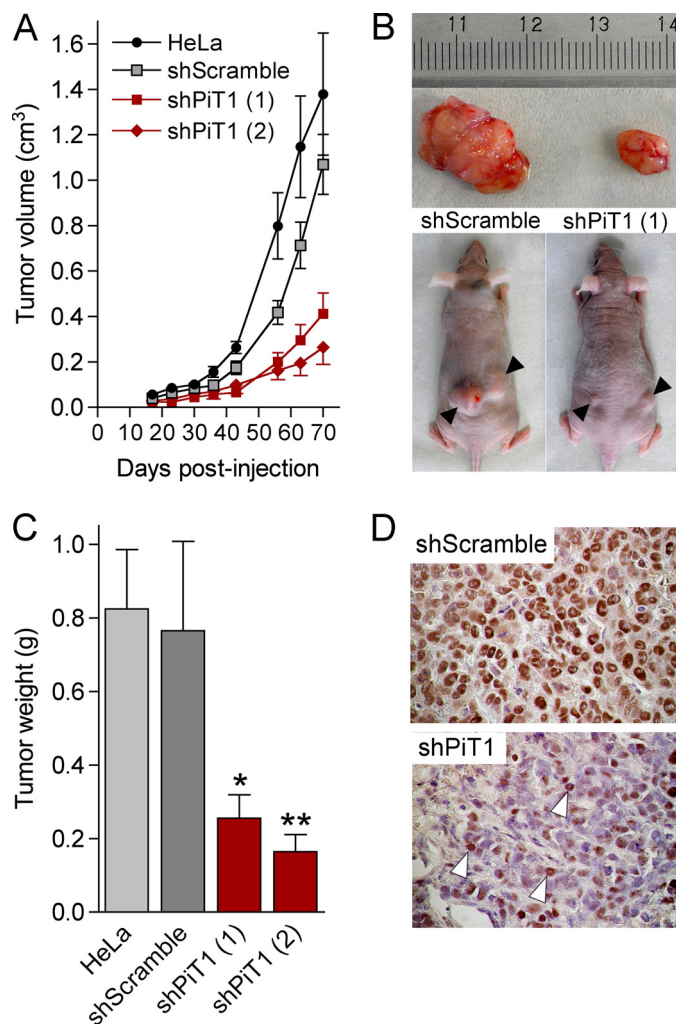
FIGURE 6. **PiT1 depletion in HeLa cells reduces tumor growth in nude mice.** Subcutaneous injection of stably transfected shPiT1 HeLa cells in nude mice (5 × 10⁶ cells) resulted in tumor formation at a similar occurrence as shScramble HeLa cells, but the tumor growth rate (*A*), tumor size (*B*), tumor weight (*C*), and proportion of PCNA-positive cells in tumor sections (*D*) at sacrifice time (70 days after implantation) were severely reduced. *, $p < 0.05$, **, $p < 0.01$. *Error bars* indicate S.E.

FIGURE 7. **RNAi-resistant PiT1 mutants rescue cell morphology, proliferation, and transport of PiT1-depleted HeLa cells.** Stable expression of a siRNA cleavage-resistant version of PiT1 (*PiT1-RNAiR*) in stably transfected shPiT1 HeLa cells rescues normal cell morphology (*A*), cell proliferation (*B*), and Na⁺-Pᵢ transport across the cell membrane (*C*). *, $p < 0.05$, **, $p < 0.01$. *Error bars* indicate S.E.

(23, 24). A recent study providing a thorough investigation of PiT1 transport properties shows that the apparent K_m for P_i was independent of the test potential, suggesting that P_i did not interact with the transmembrane electric field (18). Similarly, the maximum electrogenic activity ($I_{P_i}^{max}$) showed a rectifying behavior with no evidence of rate-limiting behavior at the hyperpolarizing limit (18). Although a specific study is required, this may indicate that the activity of PiT1 may only be slightly influenced by membrane potential, meaning that the PiT-mediated P_i transport may not be related to the proliferation state of the cell. Consistent with this hypothesis, we show that decreasing Na⁺-P_i transport does not decrease cell proliferation *per se* because cells displaying different V_{max} for P_i could proliferate at the same rate, providing that they have a normal PiT1 expression.

Our work identifying a novel function of PiT1 raises questions about the physiological function of this protein. Indeed, instead of being a ubiquitous supplier of P_i for cellular needs, PiT1 could be a regulator of cell proliferation, at least in certain cell types or under certain physiological conditions. Considering the essential role of P_i in metabolic and structural processes, one might have expected that a proliferation-related role of PiT1 would have been in relation to its P_i transport function. We show that this is not the case. The quantity of P_i molecules transported by the high affinity low capacity Na⁺-P_i transporter PiT1 may actually not represent the bulk of P_i necessary for cellular needs, and alternative large capacity low affinity P_i transporters may exist, as described for renal cells (25, 26). Hence, although PiT proteins do possess the ability to transport P_i, their main physiological functions may not be to provide cells with a sufficient amount of inorganic phosphate. In line with this hypothesis, it has been shown previously that transport-deficient mutants of PiT2
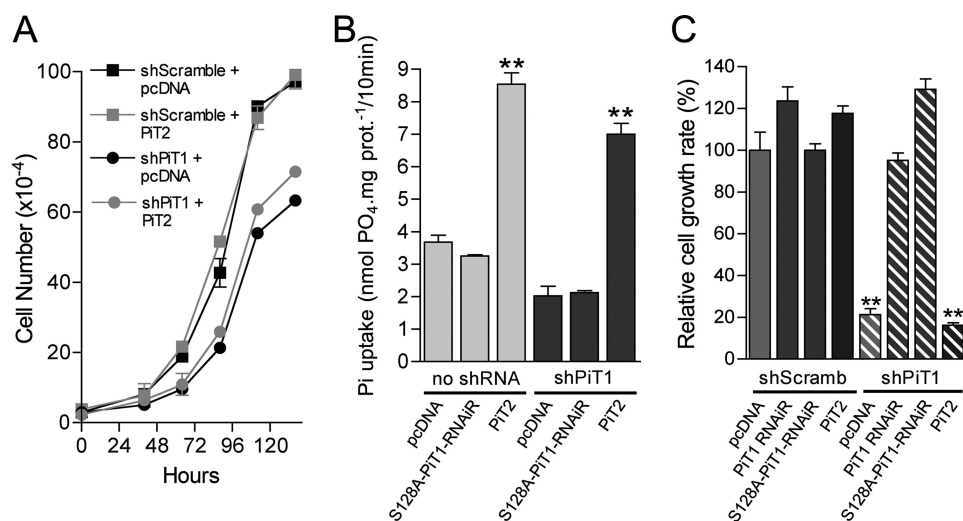
FIGURE 8. **Reduced proliferation following PiT1 inactivation is independent from Na⁺-Pᵢ transport.** *A*, stable expression of a PiT2-expressing plasmid in shPiT1 HeLa cells is unable to rescue the proliferation of PiT1-depleted cells to a normal value. *Error bars* indicate S.E. *B*, when serine at position 128 was replaced with an alanine by site-directed mutagenesis, the mutated version of PiT1 was unable to transport Pᵢ. On the contrary, expression of PiT2 leads to a 2–3-fold increase in the Na⁺-Pᵢ transport activity. *C*, transfection of the transport-deficient S128A-PiT1-RNAiR mutant in shPiT1-depleted cells rescues the cell proliferation rate, whereas overexpression of PiT2 does not. **, $p < 0.01$.
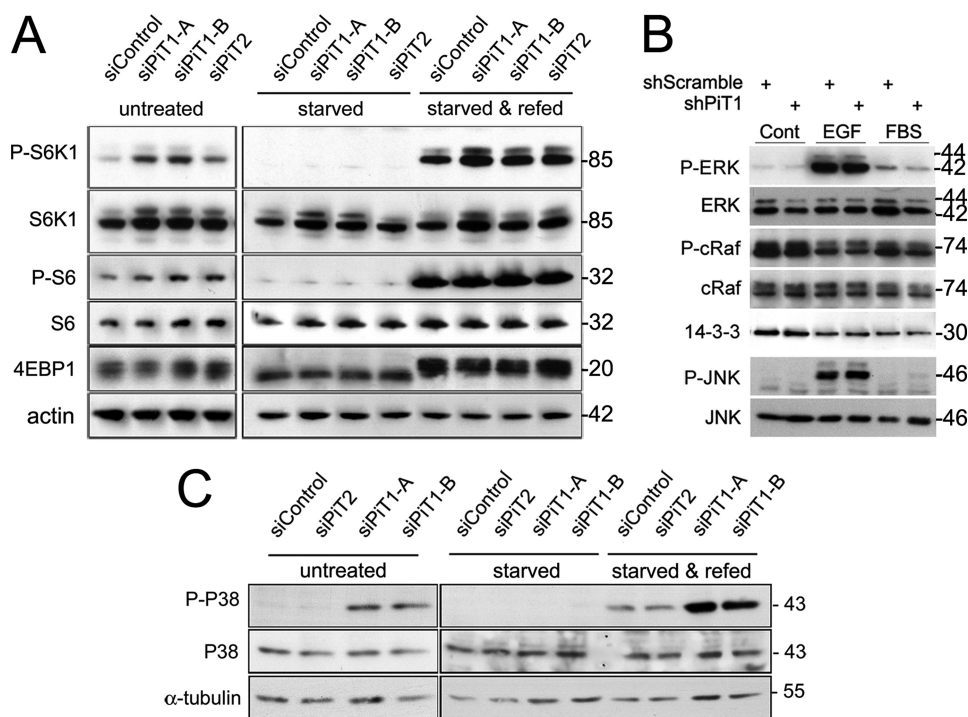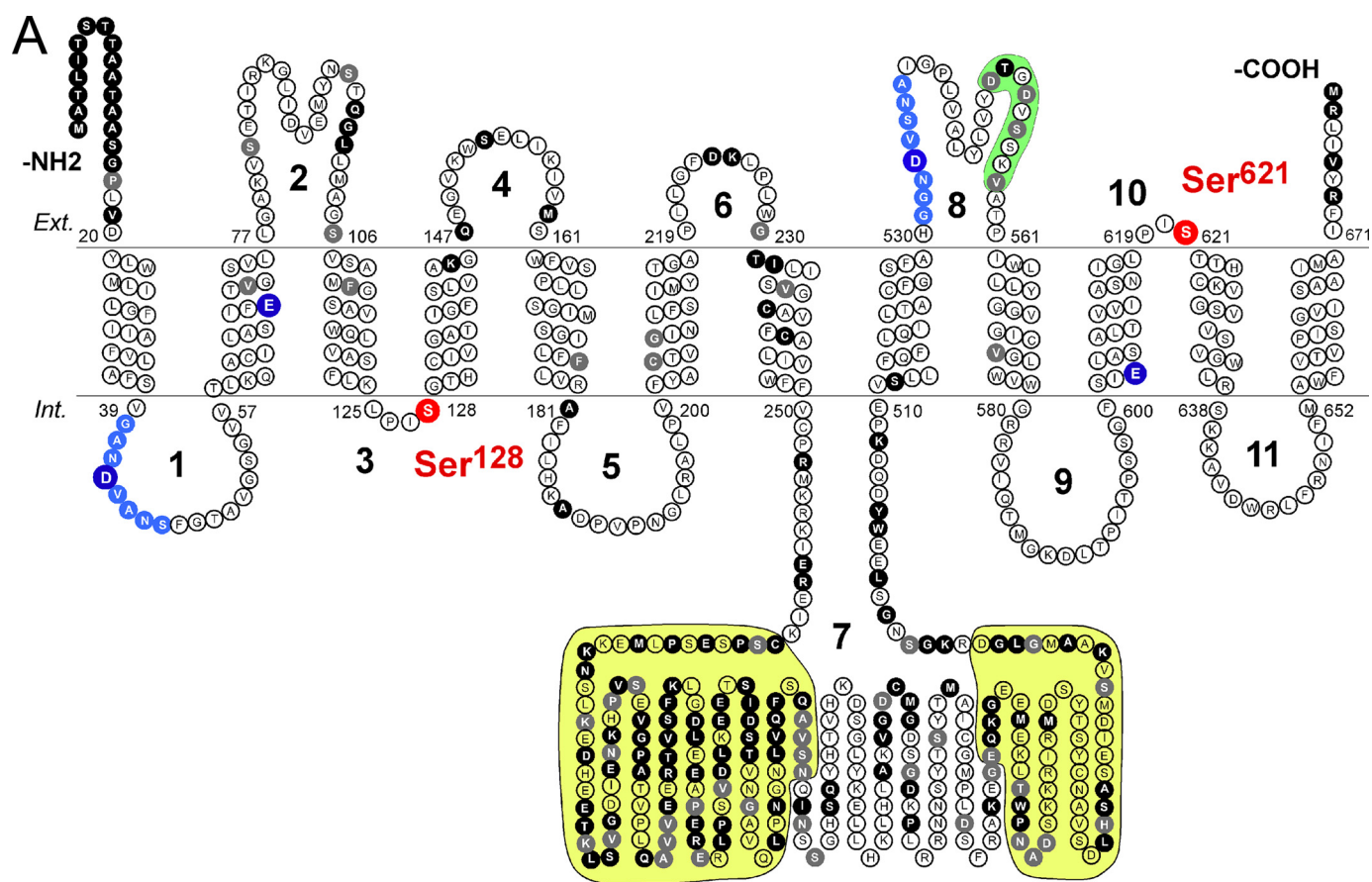

FIGURE 9. **Increased phosphorylation status of p38 MAPK in PiT1-depleted HeLa cells.** Proteins from HeLa cells were extracted from control (siControl or shScramble) and cells transfected with siRNAs or shRNAs, as indicated. Western blotting was performed using antibodies as indicated. *A*, the phosphorylation (indicated by *P*) of partners of the S6K/mTOR pathway in PiT1 or PiT2 transiently depleted cells following serum starvation and refeeding by FBS or 10 nM epidermal growth factor, was unchanged. *B*, similarly, no change was observed in the phosphorylation of ERK, c-Raf, 14-3-3σ, or JNK proteins after stimulation of PiT1-depleted HeLa cells with 10 nM epidermal growth factor (*EGF*) or 10% FBS. *C*, on the contrary, p38 was more phosphorylated in PiT1-depleted cells using two different siRNAs, either in basal conditions (*left*) or following 16 h of starvation and 30 min of refeeding by 10% FBS (*right*).

(27), there are almost no reports regarding its role in this organ *in vivo* apart from the study of Palmer *et al.* (28) showing that the expression of *PiT1* during mouse development starts during late stages and in a very precise subset of specialized cells. This is in contrast with the tremendous Pᵢ requirements of bone, where 80–85% of total Pᵢ of the body accumulates (6), and raises questions about the role of PiT1 *in vivo*.

Although PiT1 and PiT2 expression are found in a vast majority of organ and cell types, their relative tissue distributions illustrate that these two transporters may have distinct and possibly non-redundant roles *in vivo* (5, 7). In line with this hypothesis, data from the Gene Expression Omnibus (GEO) data bank (29, 30) show that *PiT1/PiT2* expression ratios were much higher in tissues with high proliferation rates and cellular turnover under physiological conditions, such as placenta, intestine, or trachea. Alignment of protein sequences of PiT family members throughout all kingdoms reveals highly conserved regions, which where assigned to the Na⁺-Pᵢ transport activity (31). Analysis of these alignments also reveals that the largest sequence differences between PiT1 and PiT2 are evident in the large intracellular loop (assuming that PiT1 and PiT2 have a comparable topology, discussed in Ref. 31). This PiT1 loop displays only 34% identity, whereas the rest of the protein shares 75% identity with PiT2 (Fig. 10). Large regions of this loop are absent from members of the PiT family from plants and bacteria (Fig. 10), suggesting a non-essential role of this region in Pᵢ transport. Whether this intracellular loop bears a specialized function and whether this function could be related to the new function that we identified for PiT1 require further investigation. To our knowledge, there is only one example in

the literature of a multispanning membrane protein that shares similar characteristics. Like PiT1 and PiT2, the GLUT2 glucose transporter displays 12 transmembrane domains and a large central intracellular loop (32). Its primary role is to transport glucose into the cell, where it is metabolized. Guillemain *et al.*

were still able to respond to external Pᵢ variations, suggesting that the PiT2 protein may function as a Pᵢ sensor besides being a Na⁺-Pᵢ transporter (20). Similarly, it is surprising to note that although there is abundant literature showing the importance of PiT1 in the biology of bone- and cartilage-forming cells *in vitro*

FIGURE 10. **The serine 128 and 621 mutants of PiT1 are correctly expressed in HeLa cells.** *A*, putative topological model for human PIT1. Transmembrane domains were assigned using the TmPred algorithm and according to Refs. 10 and 31. Serine residues important for PiT1 transport function are depicted in *red*. Other residues (Asp-43, Glu-70, Asp-534, and Glu-603) indicated in *blue* are conserved residues corresponding to those that have been shown to be essential for transport function of PiT2 (31, 38) but have not been investigated for PiT1 transport function. Conserved GANDVANA signature sequences critical for transport (31) are indicated in *light blue*. *Light green shading* indicates the region important for GALV binding (39). *Yellow shading* indicates the regions that are not present in members of the PiT family from plants and bacteria. Extensive discussion on PiT topology can be found in Refs. 31 and 27. *Ext.*, extracellular; *Int.*, intracellular. *B*, stable expression of a cleavage-resistant version of PiT1 (PiT1-RNAiR) in shPiT1 HeLa cells. Immunofluorescence on living cells shows that S128A and S621A mutants of PiT1 are expressed at the plasma membrane of HeLa cells. *C*, Western blot analysis of serine mutants of PiT1 shows that they are expressed at a level comparable with the parent version of PiT1.

(33) elegantly showed that the intracellular loop of GLUT2 could convey a glucose signal from the plasma membrane to the nucleus. Our data show that when PiT1 is depleted from the cell, there is an increase in the phosphorylation status of p38 MAPK. These results are in line with the reported key role of p38 in delaying the G_2/M transition (34, 35) under various environmental stress conditions and the inhibitory roles in cell proliferation and tumor progression (36). Moreover, our results obtained under basal culture conditions are consistent with a recent report showing that p38 could regulate the timing of mitotic entry under non-stress conditions (37). Despite these

facts, we were unable to rescue the decrease in proliferation following PiT1 depletion by blocking p38 activity or synthesis, arguing against a direct role of p38 in the PiT1-mediated effect on cell proliferation.

In conclusion, we have identified PiT1 as a critical protein for cell proliferation. This constitutes a novel function, as this effect does not stem from the Na^+-P_i cotransport activity of PiT1. We show that this function is specific to PiT1 because PiT2 does not share this function. Although p38 MAPK shows an increase in phosphorylation status, the mechanisms by which PiT1 modulates cell proliferation require further inves-

tigation, notably through the identification of PiT1 protein partners.

REFERENCES

1. Saier, M. H., Jr. (2000) *Microbiol. Mol. Biol. Rev.* **64,** 354–411
2. Werner, A., and Kinne, R. K. (2001) *Am. J. Physiol. Regul. Integr. Comp. Physiol.* **280,** R301–R312
3. O'Hara, B., Johann, S. V., Klinger, H. P., Blair, D. G., Rubinson, H., Dunn, K. J., Sass, P., Vitek, S. M., and Robins, T. (1990) *Cell Growth Differ.* **1,** 119–127
4. Miller, D. G., Edwards, R. H., and Miller, A. D. (1994) *Proc. Natl. Acad. Sci. U.S.A.* **91,** 78–82
5. Kavanaugh, M. P., Miller, D. G., Zhang, W., Law, W., Kozak, S. L., Kabat, D., and Miller, A. D. (1994) *Proc. Natl. Acad. Sci. U.S.A.* **91,** 7071–7075
6. Crook, M., and Swaminathan, R. (1996) *Ann. Clin. Biochem.* **33,** 376–396
7. Uckert, W., Willimsky, G., Pedersen, F. S., Blankenstein, T., and Pedersen, L. (1998) *Hum. Gene Ther.* **9,** 2619–2627
8. Chien, M. L., Foster, J. L., Douglas, J. L., and Garcia, J. V. (1997) *J. Virol.* **71,** 4564–4570
9. Brummelkamp, T. R., Bernards, R., and Agami, R. (2002) *Science* **296,** 550–553
10. Salaün, C., Rodrigues, P., and Heard, J. M. (2001) *J. Virol.* **75,** 5584–5592
11. Beck, L., and Markovich, D. (2000) *J. Biol. Chem.* **275,** 11880–11890
12. Livak, K. J., and Schmittgen, T. D. (2001) *Methods* **25,** 402–408
13. Escoubet, B., Silve, C., Balsan, S., and Amiel, C. (1992) *J. Endocrinol.* **133,** 301–309
14. Whitfield, M. L., Zheng, L. X., Baldwin, A., Ohta, T., Hurt, M. M., and Marzluff, W. F. (2000) *Mol. Cell. Biol.* **20,** 4188–4198
15. Tomayko, M. M., and Reynolds, C. P. (1989) *Cancer Chemother. Pharmacol.* **24,** 148–154
16. Prié, D., Ureña Torres, P., and Friedlander, G. (2009) *Kidney Int.* **75,** 882–889
17. Ross, D. T., Scherf, U., Eisen, M. B., Perou, C. M., Rees, C., Spellman, P., Iyer, V., Jeffrey, S. S., Van de Rijn, M., Waltham, M., Pergamenschikov, A.,
18. Ravera, S., Virkki, L. V., Murer, H., and Forster, I. C. (2007) *Am. J. Physiol. Cell Physiol.* **293,** C606–C620
19. Bøttger, P., Hede, S. E., Grunnet, M., Høyer, B., Klaerke, D. A., and Pedersen, L. (2006) *Am. J. Physiol. Cell Physiol.* **291,** C1377–C1387
20. Salaün, C., Maréchal, V., and Heard, J. M. (2004) *J. Mol. Biol.* **340,** 39–47
21. Fingar, D. C., Richardson, C. J., Tee, A. R., Cheatham, L., Tsou, C., and Blenis, J. (2004) *Mol. Cell. Biol.* **24,** 200–216
22. Sundelacruz, S., Levin, M., and Kaplan, D. L. (2009) *Stem Cell Rev. Rep.* **5,** 231–246
23. Binggeli, R., and Weinstein, R. C. (1986) *J. Theor. Biol.* **123,** 377–401
24. Cone, C. D., Jr. (1971) *J. Theor. Biol.* **30,** 151–181
25. Tenenhouse, H. S., Klugerman, A. H., and Neal, J. L. (1989) *Biochim. Biophys. Acta* **984,** 207–213
26. Barac-Nieto, M., Alfred, M., and Spitzer, A. (2001) *Exp. Nephrol.* **9,** 258–264
27. Virkki, L. V., Biber, J., Murer, H., and Forster, I. C. (2007) *Am. J. Physiol. Renal Physiol.* **293,** F643–F654
28. Palmer, G., Zhao, J., Bonjour, J., Hofstetter, W., and Caverzasio, J. (1999) *Bone* **24,** 1–7
29. Barrett, T., Troup, D. B., Wilhite, S. E., Ledoux, P., Rudnev, D., Evangelista, C., Kim, I. F., Soboleva, A., Tomashevsky, M., and Edgar, R. (2007) *Nucleic Acids Res.* **35,** D760–D765
30. Su, A. I., Wiltshire, T., Batalov, S., Lapp, H., Ching, K. A., Block, D., Zhang, J., Soden, R., Hayakawa, M., Kreiman, G., Cooke, M. P., Walker, J. R., and Hogenesch, J. B. (2004) *Proc. Natl. Acad. Sci. U.S.A.* **101,** 6062–6067
31. Bøttger, P., and Pedersen, L. (2005) *FEBS J.* **272,** 3060–3074
32. Thorens, B., Sarkar, H. K., Kaback, H. R., and Lodish, H. F. (1988) *Cell* **55,** 281–290
33. Guillemain, G., Loizeau, M., Pinçon-Raymond, M., Girard, J., and Leturque, A. (2000) *J. Cell Sci.* **113,** 841–847
34. Bulavin, D. V., Higashimoto, Y., Popoff, I. J., Gaarde, W. A., Basrur, V., Potapova, O., Appella, E., and Fornace, A. J., Jr. (2001) *Nature* **411,** 102–107
35. Reinhardt, H. C., Aslanian, A. S., Lees, J. A., and Yaffe, M. B. (2007) *Cancer Cell* **11,** 175–189
36. Hui, L., Bakiri, L., Mairhorfer, A., Schweifer, N., Haslinger, C., Kenner, L., Komnenovic, V., Scheuch, H., Beug, H., and Wagner, E. F. (2007) *Nat. Genet.* **39,** 741–749
37. Cha, H., Wang, X., Li, H., and Fornace, A. J., Jr. (2007) *J. Biol. Chem.* **282,** 22984–22992
38. Bottger, P., and Pedersen, L. (2002) *J. Biol. Chem.* **277,** 42741–42747
39. Dreyer, K., Pedersen, F. S., and Pedersen, L. (2000) *J. Virol.* **74,** 2926–2929

Lee, J. C., Lashkari, D., Shalon, D., Myers, T. G., Weinstein, J. N., Botstein, D., and Brown, P. O. (2000) *Nat. Genet.* **24,** 227–235